Computerized Analysis of Abnormal Asymmetry in Digital Chest Radiographs: Evaluation of Potential Utility

Samuel G. Armato III, Maryellen L. Giger, and Heber MacMahon

The purpose of this study was to develop and test a computerized method for the fully automated analysis of abnormal asymmetry in digital posteroanterior (PA) chest radiographs. An automated lung segmentation method was used to identify the aerated lung regions in 600 chest radiographs. Minimal *a priori* lung morphology information was required for this gray-level thresholding-based segmentation. Consequently, segmentation was applicable to grossly abnormal cases. The relative areas of segmented right and left lung regions in each image were compared with the corresponding area distributions of normal images to determine the presence of abnormal asymmetry. Computerized diagnoses were compared with image ratings assigned by a radiologist. The ability of the automated method to distinguish normal from asymmetrically abnormal cases was evaluated by using receiver operating characteristic (ROC) analysis, which yielded an area under the ROC curve of 0.84. This automated method demonstrated promising performance in its ability to detect abnormal asymmetry in PA chest images. We believe this method could play a role in a picture archiving and communications (PACS) environment to immediately identify abnormal cases and to function as one component of a multifaceted computer-aided diagnostic scheme.

KEY WORDS: computer-aided diagnosis, lung segmentation, gross abnormality, chest radiography.

AUTOMATED SEGMENTATION of anatomic regions in digital radiographs is a key element of computer-aided diagnostic (CAD) methods. In chest radiography, investigators are developing methods to identify intercostal spaces,[1] rib borders,[2-4] ribcage margins,[5] hemidiaphragm borders,[6] costophrenic angles,[7] and the complete lung boundary.[8-14] We have developed a computerized method for the automated segmentation of the aerated lung fields in digital posteroanterior (PA) chest radiographs.[14] This method is based on gray-level thresholding techniques, including iterative global gray-level thresholding and local gray-level thresholding, which reduce the need for *a priori* assumptions regarding the overall morphology of the lung regions. Consequently, this method is particularly robust when applied to grossly abnormal images, which may be caused by dense infiltrates, substantial pleural effusions, large neoplasms, extensive atelectasis, thoracotomy, elevated hemidiaphragm, or asymmetric cardiomegaly. These conditions may affect lung volume to such an extent that a large-scale opacity is demonstrated on the radiograph, thereby reducing the area of and altering the morphology of the aerated lung as projected on the image plane.

With the exception of interval change detection,[15] most CAD schemes currently being developed for digital chest radiography are specific to one particular pathology.[16-24] These schemes often utilize information regarding the "normal" appearance of the ribcage, diaphragm, and mediastinum in a chest image. A potential problem arises when the nature of the thoracic abnormality is such that it substantially affects the volume of the lungs. A large-scale abnormality of this type may present radiographically as abnormal asymmetry, which occurs when a gross abnormality is demonstrated in only one hemithorax (or is more extensive in one hemithorax than in the other). This can substantially alter the overall morphology of the thorax, which, while apparent to a radiologist, could result in the failure of computerized schemes.

The gray-level thresholding-based lung segmentation scheme, however, may be used to detect the presence of abnormal asymmetry.[25] The computer-extracted lung segmentation contours are expected to appropriately exclude radio-opaque regions that impinge on the lung field and encompass only the remaining aerated region. Consequently, areas of the right and left lung segmentation contours correspond to the projected areas of the aerated lung regions. The lung segmentation contours are

From the Kurt Rossmann Laboratories for Radiologic Image Research, Department of Radiology, The University of Chicago.
Supported in part by USPHS Grants CA48985, T32 CA09649, AR42739, and CA64370.
M.L. Giger and H. MacMahon are shareholders in R2 Technology, Inc. (Los Altos, CA). (It is the policy of the University of Chicago that investigators disclose publicly actual or potential significant financial interest which would reasonably appear to be directly and significantly affected by the research activities.)
Address reprint requests to Samuel G. Armato III, PhD, Kurt Rossmann Laboratories, Department of Radiology, MC 2026, The University of Chicago, 5841 S Maryland Ave, Chicago, IL 60637.

0897-1889/99/1201-0002$10.00/0

used to automatically determine these projected areas, from which two measures of asymmetry are calculated. Substantial deviation of these measures from the measures determined for a set of normal images indicates the presence of abnormal asymmetry.

The detection scheme presented here could be implemented as part of a picture archiving and communications system (PACS)[26] in a digital radiology department as a computerized triage and prioritization system, so that the images of patients with severe abnormalities may be brought to the immediate attention of radiologists. Moreover, since the segmentation scheme is sensitive to a wide range of pathologic conditions, it may be applied to images prior to other more lesion-specific computerized schemes that may fail if attempted on a grossly abnormal case. Symmetric abnormalities, however, would not be detected in this manner; further information on absolute lung areas would be required.

MATERIALS AND METHODS

Lung Segmentation

We compiled a database of 600 clinical PA chest images extracted from databases of radiographs collected by others.[5,15,27] All radiographs were acquired with a Thoramat (Siemens; Munich, Germany) dedicated chest radiography unit, using a Lanex Medium OC (Eastman Kodak Co; Rochester, NY) screen-film system at 125 kVp with a 12:1 focused grid and a 183 cm source-to-film distance. In all cases the patients were imaged with 14- × 17-in (35.6 × 43.2-cm) vertically oriented film. The radiographs were digitized at 10-bits of gray scale using a laser film scanner (KFDR-S; Konica Corp; Tokyo, Japan), which assigned low pixel values to regions of high optical density and high pixel values to regions of low optical density. The images were spatially subsampled to obtain a working image matrix size of 286 × 347 pixels (1.2-mm pixel dimension).

Detection of abnormal asymmetry begins with automated segmentation of the aerated lung regions, a method that has been reported previously.[14] To summarize, a gray-level histogram is constructed from the central portion of the image. The maxima and minimum of this typically bimodal histogram are used to identify a range of gray levels that will be utilized during the iterative global gray-level thresholding process. At each gray-level thresholding iteration, a binary image is constructed in which only pixels with a corresponding image pixel gray level less than the threshold are turned "on," and contours are constructed around each group of contiguous "on" pixels. Horizontal gray-level profile analysis is performed on each of these groups to eliminate regions external to the lungs. Consequently, regions outside the lungs are unable to merge with lung regions, a likely occurrence at later iterations. With each subsequent iteration, the gray-level threshold is increased, and the procedure is repeated. In this manner, the segmentation contours effectively expand to encompass the aerated portion of the lung regions. Local gray-level thresholding is then implemented within a series of regions-of-interest (ROIs) to more completely capture the aerated lung regions. A final contour set is constructed based on a composite binary image created by thresholding pixels within individual local ROIs. Lung segmentation is complete after costophrenic angle delineation is performed.[7]

Areas of the final lung segmentation contours are computed from the numbers of image pixels included within the contours. These computer-extracted areas, which correspond to the projected areas of the aerated lung regions, are used to calculate measures of asymmetry from which the presence of an abnormality is determined. The right lung area and left lung area are defined as the sum of the areas of all contours on the corresponding side of the mediastinum. Presumably, all contours outside the lung regions have been suppressed, and large abnormalities may divide the aerated portion of one lung into two or more regions. Figure 1 shows the segmentation contours encompassing the aerated lung regions of an image with abnormal asymmetry caused by an elevated left hemidiaphragm.

Measures of Asymmetry

Two measures are used to assess abnormal asymmetry: (1) the "ratio measure," and (2) the "distance measure."[25] Both measures require comparison with values for known normal images. Consequently, the measures are based on the right and left lung areas, computed by the segmentation scheme, for a set of radiographically normal images (the "baseline normal images").

The first measure of asymmetry, the "ratio measure," utilizes the mean and standard deviation of the right-lung-area-to-left-lung-area ratio for the baseline normal images. This mean ratio is greater than one because the cardiac silhouette impinges on the projected area of the left lung. For all other images in the database not included in the set of baseline normal images, the ratio of right and left lung areas is computed. A decision regarding the presence of abnormal asymmetry for a particular image is based on the difference between the area ratio associated with that image and the mean baseline normal ratio; abnormal cases are expected to result in greater differences than normal cases.

The second measure of asymmetry is based on a graphical comparison of lung areas. For the same set of baseline normal images, the left lung area is plotted as a function of right lung area for each image. A regression line[28] is then constructed from these points (Fig 2). The "distance measure" utilizes the mean and standard deviation of the perpendicular distance from this regression line to the baseline normal image points. The perpendicular distance associated with a representative baseline normal image point is indicated by "d" in Fig 2. Left lung area is then plotted against right lung area for all other images in the database. The decision variable is the perpendicular distance from the regression line of baseline normals to the point representing a particular image. It is expected that this distance will be greater for a case with abnormal asymmetry, since such a case will exhibit a reduction in aerated area of one lung relative to the other.

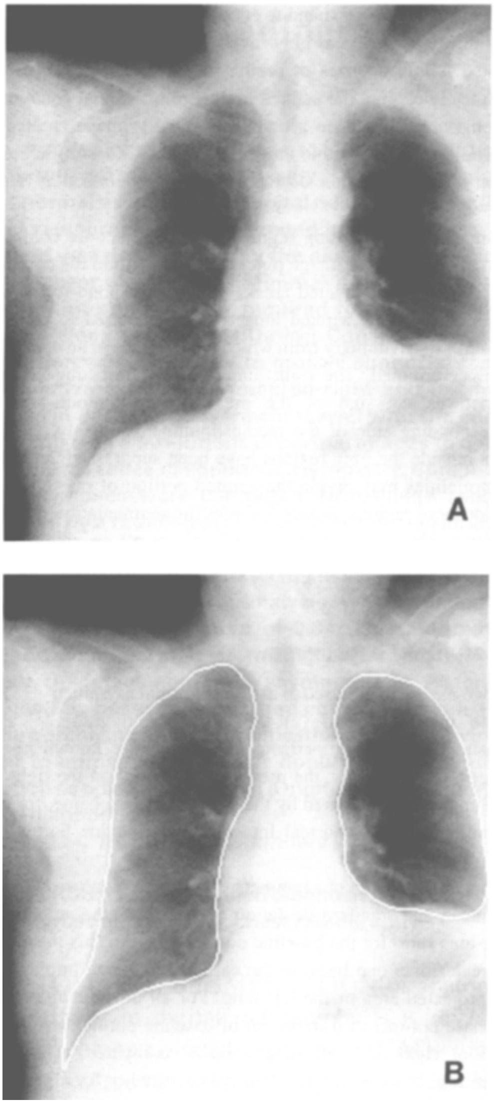

Fig 1. (A) Original image and (B) the image with its computer-determined contours overlaid in a case demonstrating an elevated left hemidiaphragm.

Subjective Evaluation of Abnormality

An abnormality has, in the present context, two defining global characteristics, namely, the area it occupies as projected onto the image plane and its radiolucency. A diffuse infiltrate may occupy a substantial fraction of one lung, but its overall optical density might not be much lower than the surrounding unaffected parenchyma. Conversely, a dense lesion may be quite small compared to the overall dimension of the lung region, as in the case of a calcified granuloma. Both aspects of an abnormality should be considered to assess abnormal asymmetry.

Although determining the presence of an abnormality in an image is, in a simplistic sense, effectively a binary decision (ie, calling the case normal or abnormal), the present situation requires a judgment as to whether the abnormality is gross enough to constitute abnormal asymmetry in the image. For example, the presence of a granuloma renders a case abnormal, but its radiographic effect will not produce what we have defined as abnormal asymmetry. On the other side of the spectrum, a patient who has had a pneumonectomy will typically demonstrate a completely radio-opaque hemithorax, which yields the most extreme condition of asymmetry. Accordingly, a subjective rating system was established to assess the area occupied by an abnormality in each hemithorax along with the opacity of that abnormality.

The images in the database were reviewed by an attending chest radiologist [HM] to assess the degree to which abnormalities existed and thereby establish "truth." Each image was displayed on an Indy Workstation (Silicon Graphics, Inc; Mountain View, CA). Each hemithorax of each image was evaluated using one rating scale for the projected area occupied by an abnormality (0 = normal, 1 = less than 25% of the lung area affected, 2 = 25% to 50% of the lung area affected, 3 = more than 50% of the lung area affected) and another rating scale for the opacity of the abnormal region (0 = normal, 1 = minimal opacity, 2 = intermediate opacity, 3 = complete opacity). For example, the left hemithorax of Fig 1 was assigned an area rating of 2 and an opacity rating of 3, while the right hemithorax was evaluated as normal (0 for both ratings). It is important to note that hemithoraces classified as "normal" were normal with respect to abnormalities that substantially impinged on the aerated lung area. According to this criterion, focal scarring or small lung nodules, for example, were ignored as abnormalities. In other words, an area rating of 1 (less than 25%) was assigned only when the extent of an abnormality exceeded some subjective threshold.

Figure 3A presents the distributions of area and opacity ratings assigned to all 600 images in the database (1200 hemithoraces). Figure 3B shows the distributions of the area and opacity ratings assigned to hemithoraces in images that were not normal; these data correspond to images in which at least one

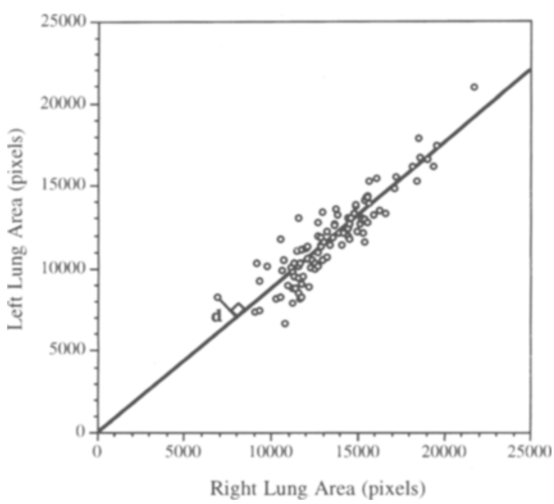

Fig 2. Plot of left lung area versus right lung area for the 100 baseline normal images. The regression line is also shown. "d" represents the perpendicular distance from the regression line of a representative point and is the basis of the distance measure.

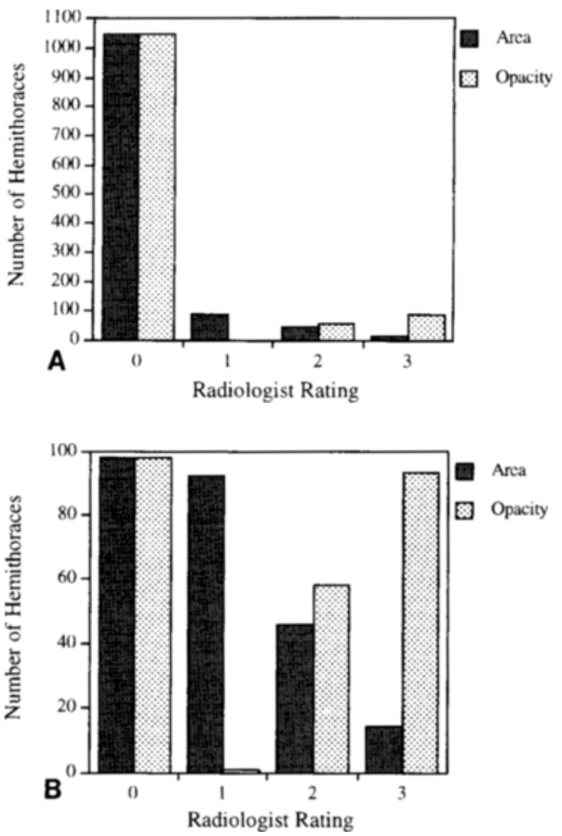

Fig 3. Histograms of radiologist ratings assigned to the area and opacity of abnormality. (A) Ratings for all 1200 hemithoraces. (B) Ratings for 250 hemithoraces from only those cases demonstrating an abnormality in at least one hemithorax.

hemithorax was assigned a non-zero rating for "area of abnormality." Of the 600 images, 475 were classified as normal (ie, area rating equals 0 for both hemithoraces), and 125 were abnormal (ie, a non-zero area rating assigned to at least one hemithorax). It is important to note that this definition does not incorporate any measure of asymmetry between the hemithoraces.

Baseline Normal Images

The lung areas as calculated by the automated lung segmentation method were used to construct the abnormal asymmetry measures previously discussed. Both the ratio measure and the distance measure require a set of baseline normal images to establish the average right-lung-area-to-left-lung-area ratio and the regression line, respectively, for normal cases. The first 100 images in the database (in case-number order) to satisfy the following two criteria were selected as the baseline normals: (1) area and opacity ratings of 0 (ie, normal) for both hemithoraces as assigned by the reviewing radiologist (an ancillary costophrenic angle rating of "normal" was also required), and (2) computer-determined lung segmentation contours rated as either moderately or highly accurate by two evaluating radiologists as part of a separate study.[14] This last requirement was consistent with our intended goal: since the detection of abnormal asymmetry utilizes lung area information that results from the automated lung segmentation scheme, only the area values of normal images with accurate segmentation contributed to the "average normal ratio" and the "regression line for normals."

The basis for the ratio measure is the mean ratio of right lung area to left lung area for the baseline normal images. Figure 4 is a histogram of the lung area ratios for all 600 images in the database. Greater deviations from the calculated baseline normal image mean ratio of 1.15 ($\pm$0.12) should indicate more pronounced degrees of abnormal asymmetry. Four images with lung area ratios greater than 2.30 are not represented in the histogram.

As discussed previously, Fig 2 presents a plot of left lung area as a function of right lung area for the 100 baseline normal images along with the corresponding regression line. The distance measure is based on the mean perpendicular distance of baseline normal image points from the regression line, the equation of which is given by

$$\text{(left lung area)} = 0.88\ \text{(right lung area)} - 70.38$$

The mean perpendicular distance of baseline normal points from the regression line was 643.0 $\pm$ 489.4 pixels. Figure 5 presents a plot of left lung area as a function of right lung area for all 600 images. The regression line for baseline normal images is shown along with two parallel lines representing the mean distance (643 pixels) of baseline normal points from the regression line. Abnormal images are not distinguished from normal images in this plot, because multiple definitions of "abnormal" were used in the evaluation as discussed below.

RESULTS

Receiver operating characteristic (ROC) analysis[29] was used to assess the ability of the abnormal asymmetry detection scheme to distinguish between images with and without abnormal asymmetry by using the LABROC4 software package (C.E. Metz, PhD, The University of Chicago).[30] The area under the ROC curve (A_Z) served as the index of performance. Four different measures of abnormality were used, namely, the ratio measure alone, the distance measure alone, a measure consisting of a logical AND operation between the ratio and distance measures (ie, *both* measures need to exceed the critical value of the decision variable in order for a case to be called "abnormal"), and a measure consisting of a logical OR operation between the ratio and distance measures (ie, a case is called "abnormal" if *either* measure exceeds the critical value). Moreover, several different definitions of a "true" abnormal case were used to assess the ability of the scheme to detect abnormal asymmetry of varying degrees. For each combination of asymmetry measure and "truth" definition, the scheme was applied first to all 600 images (including the 100 baseline normal cases) and then to the 500 images that remained after exclusion of

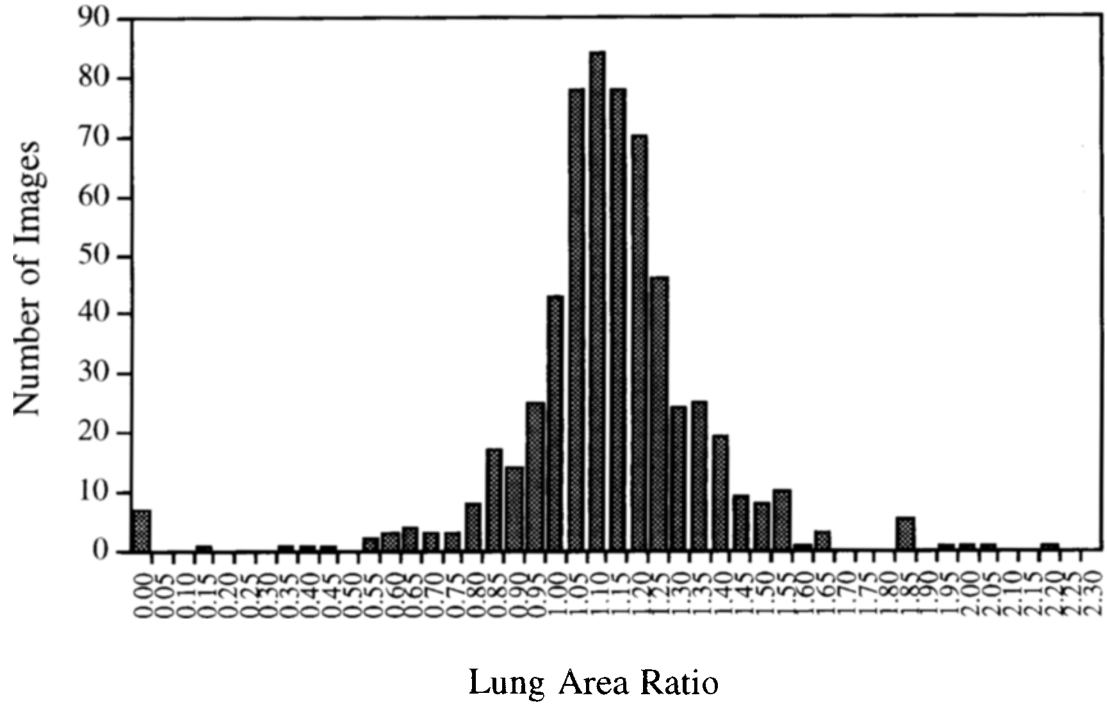

Fig 4. Histogram of the right-lung-area-to-left-lung-area ratios for all 600 images. Greater deviations from the calculated baseline normal image mean ratio of 1.15 (±0.12) should indicate more pronounced degrees of abnormal asymmetry. Four images with lung area ratios greater than 2.30 are not depicted.

the baseline normal images (to separate "training" from "testing" cases).

Table 1 presents A_Z for the various combinations of asymmetry measure and "truth" definition. The numbers of images considered to be "true" normals and "true" abnormals for each definition of "truth" are indicated. The ratio measure yielded the highest A_Z value for all conditions, with slightly lower values occurring when baseline normal cases were excluded from the testing phase. In general, performance increased as the opacity rating increased or as the difference between the area ratings for the two hemithoraces increased. Figure 6 presents ROC curves of ratio measure performance for four of the conditions in Table 1.

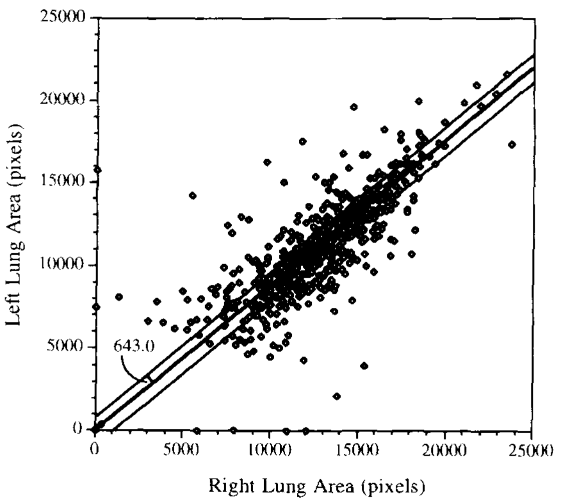

Fig 5. Plot of left lung area versus right lung area for all 600 images. The regression line for baseline normal images is shown along with two parallel lines representing the mean distance of baseline normal points from the regression line. Abnormal images are not distinguished from normal images in this plot, because abnormality can be defined in different ways.

DISCUSSION

Selection of the baseline normal cases and calculation of their associated measures (ie, ratio of right lung area to left lung area and distance from the left lung area versus right lung area regression line) is an important aspect of this method, because the criteria used in our analysis are calculated from these baseline normal cases. It is worthwhile to investigate the robustness of the method with regard to baseline normal case selection. The database contained 325 cases for which (1) both the area and opacity were rated as normal by the radiologist, (2) both costophrenic angles were rated

Table 1. Performance of Abnormal Asymmetry Detection Scheme Combining Different Abnormality Measures With a Range of "True" Abnormal Definitions

Definition of Abnormal	N_N	N_A	Baseline Normals Included	Abnormality Measure: Ratio	Distance	Ratio AND Distance	Ratio OR Distance
Either lung assigned non-zero area rating	475	125	yes	.79 ± .024	.74 ± .027	.76 ± .026	.78 ± .025
			no	.78 ± .024	.73 ± .028	.75 ± .027	.76 ± .026
Difference between area ratings ≥1; opacity ≥2 for more abnormal lung	492	108	yes	.79 ± .024	.74 ± .029	.76 ± .028	.77 ± .026
			no	.78 ± .025	.73 ± .030	.75 ± .029	.76 ± .027
Difference between area ratings ≥1; opacity = 3 for more abnormal lung	525	75	yes	.81 ± .026	.73 ± .034	.76 ± .033	.80 ± .028
			no	.80 ± .027	.71 ± .035	.74 ± .033	.78 ± .029
Difference between area ratings ≥2; opacity ≥2 for more abnormal lung	570	30	yes	.79 ± .049	.74 ± .056	.75 ± .055	.79 ± .050
			no	.78 ± .050	.73 ± .057	.74 ± .056	.77 ± .051
Difference between area ratings ≥2; opacity = 3 for more abnormal lung	578	22	yes	.85 ± .046	.78 ± .060	.82 ± .055	.83 ± .052
			no	.84 ± .048	.77 ± .062	.81 ± .057	.82 ± .053
Difference between area ratings = 3; opacity of abnormal lung ≥2	592	8	yes	.99 ± .0042	.99 ± .0098	.99 ± .0055	.99 ± .0080
			no	.99 ± .0050	.99 ± .012	.99 ± .0064	.99 ± .0097

NOTE. The values reported are areas under the ROC curve for each condition. N_N and N_A refer to the number of cases considered to be normal and abnormal, respectively, according to each definition of "true" abnormal.

as normal, and (3) the computer-determined lung segmentation contours were rated as either moderately or highly accurate by two evaluating radiologists (as part of another study). The results reported in the preceding section were based on the selection of the first 100 of these cases (in case-number order) as the baseline normal cases, which will be referred to as the "standard baseline normal set." We then assessed the ability of the method to detect abnormal asymmetry with three other sets of baseline normal cases: (1) the second 100 of the 325 cases, (2) the third 100 of the 325 cases, and (3) all 325 of the cases satisfying the criteria outlined previously.

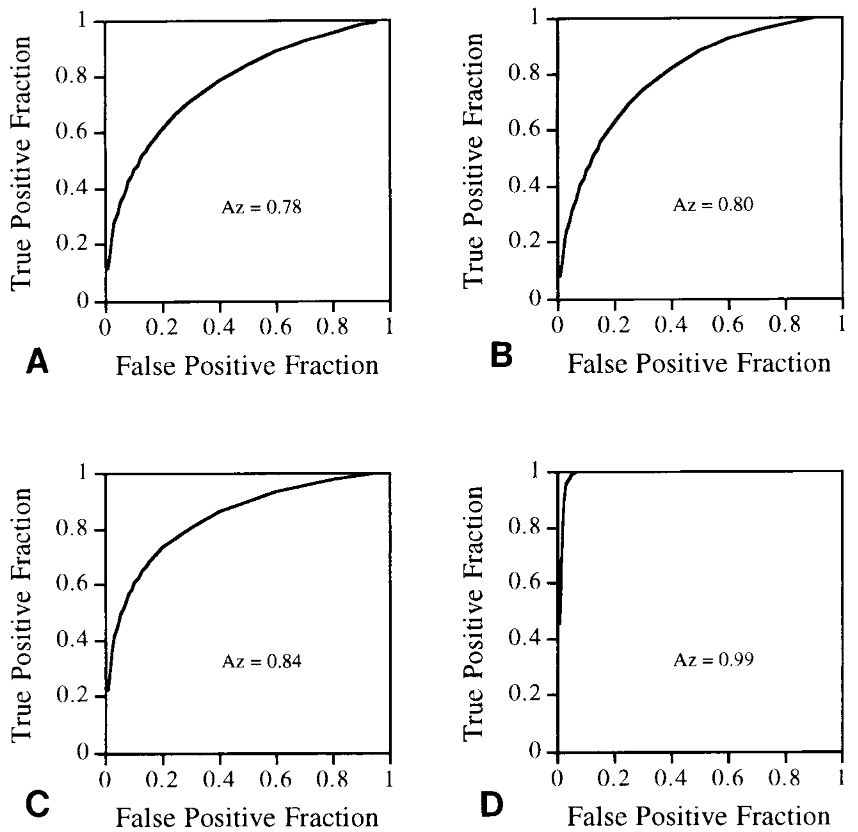

Fig 6. ROC curves for abnormal asymmetry detection based on the ratio measure. A different definition of "true" abnormal underlies each curve (see Table 1): abnormal defined as an image (A) in which either lung has a non-zero "area of abnormality" rating, (B) with different area ratings for each lung and an opacity rating = 3 for the more abnormal lung, (C) with a difference between area ratings ≥2 and opacity = 3 for the more abnormal lung, (D) with a difference between area ratings = 3 and opacity ≥2 for the more abnormal lung. The baseline normal images were not included in the analyses generating these curves.

Table 2. Mean Ratio of Right Lung Area to Left Lung Area and Mean Distance From the Regression Line for Four Sets of Baseline Normal Cases

Baseline Normals Selected	Ratio	*P*	Distance	*P*
First 100 of the 325 cases (standard baseline normal set)	1.15 ± 0.12	—	643.0 ± 489.4	—
Second 100 of the 325 cases	1.13 ± 0.11	.28	631.4 ± 525.2	.87
Third 100 of the 325 cases	1.18 ± 0.098	.07	559.0 ± 468.3	.22
All 325 cases	1.16 ± 0.11	.68	631.0 ± 501.0	.83

NOTE. The *P* values listed are based on a *t*-test comparison of the individual means with the standard baseline normal set means.

The mean right-lung-area-to-left-lung-area ratio and the mean distance from the regression line for all four sets of baseline normal cases are listed in Table 2. The *P* values listed in Table 2 are based on a two-sample *t*-test[28] comparison of the mean ratio of each of the three additional baseline normal sets with the mean ratio of the standard baseline normal set (ie, first row of the table); a similar analysis was performed for the mean distances. No statistical significance was found at the $P = .05$ level among the mean ratio values or the mean distance values of the other three sets of baseline normal cases relative to the respective means of the standard baseline normal set. Therefore, we have no evidence that the different sets of images represent distinct populations.

We then repeated the ROC analysis of the performance of the method by using the three additional sets of baseline normal cases to establish the detection criteria. Table 3 shows, in a format adapted from Table 1, the performance (ie, A_Z values) of the ratio measure based on different sets of baseline normal images. The ROCKIT software package (C.E. Metz, PhD, The University of Chicago) was used to obtain the *P* values, which are based on a comparison with the performance of the ratio measure when the standard baseline normal set is used to establish the detection criteria. No statistical significance was found at the $P = .05$

Table 3. Effect of Baseline Normal Image Selection on the Performance of the Ratio Measure in the Assessment of Abnormal Asymmetry

Definition of Abnormal	Corresponding Baseline Normals Included	Baseline Normal Selection: Standard Normal Set (First 100)	Second 100 of the 325 Cases	Third 100 of the 325 Cases	All 325 Normal Cases
Either lung assigned non-zero area rating	yes	.79	.78 $P = .24$	.79 $P = .73$	.80 $P = .82$
	no	.78	.77 $P = .54$	.77 $P = .85$	—
Difference between area ratings ≥1; opacity ≥2 for more abnormal lung	yes	.79	.79 $P = .81$	.79 $P = .60$	.80 $P = .88$
	no	.78	.77 $P = .78$	.77 $P = .47$	—
Difference between area ratings ≥1; opacity = 3 for more abnormal lung	yes	.81	.81 $P = .06$	.82 $P = .52$	.82 $P = .43$
	no	.80	.79 $P = .10$	.80 $P = .44$	—
Difference between area ratings ≥2; opacity ≥2 for more abnormal lung	yes	.79	.79 $P = .79$	.81 $P = .85$	.80 $P = .59$
	no	.78	.78 $P = .89$	.79 $P = .94$	—
Difference between area ratings ≥2; opacity = 3 for more abnormal lung	yes	.85	.85 $P = .82$	.85 $P = .41$	.85 $P = .94$
	no	.84	.83 $P = .20$	.84 $P = .93$	—
Difference between area ratings = 3; opacity of abnormal lung ≥2	yes	.99	.99 $P = 1.0$	.99 $P = 1.0$	.99 $P = 1.0$
	no	.99	.99 $P = 1.0$	.99 $P = .87$	—

NOTE. The values reported are areas under the ROC curve for each condition. The *P* values are based on a comparison with the performance of the ratio measure based on the standard baseline normal set.

level between the performance of the ratio measure based on the standard baseline normal set and the performance of the ratio measure based on any of the other three baseline normal sets. This result demonstrates the robustness of the abnormal asymmetry detection method.

Since abnormal asymmetry may present as a diffuse region of increased density (air space infiltrates, for example), comparison of lung segmentation contour areas may not be sufficient to detect the presence of an abnormality. For example, the density of a diffuse abnormality might be such that the thresholding techniques would cause the lung contour to encompass the abnormality without a reduction in contour area. To eliminate this type of false-negative, optical density information could be incorporated into the detection scheme. Such a density test could be applied to those cases labeled "normal" based on area comparison tests to achieve improved performance. Future work could also seek to establish the distribution of normal lung area ratios and normal density ratios based on analysis of a large collection of normal images. With such information, it may be possible to extend these methods to the detection of symmetrically distributed thoracic abnormalities.

The automated lung segmentation method we developed for PA chest images utilizes an iterative global gray-level thresholding scheme followed by a local gray-level thresholding scheme. Accordingly, little *a priori* information regarding the overall morphology of the aerated lung regions is required. This scheme has been adapted to detect large-scale abnormalities that occur in only one hemithorax or that are more extensive in one hemithorax relative to the other. Measures based on relative areas of the right and left lungs have been developed that allow for an automated assessment of the presence of abnormal asymmetry based on a comparison with normal cases. The advantage of this approach is its sensitivity to a wide variety of abnormalities.

ACKNOWLEDGMENT

The authors would like to thank Chunsheng Jiang, PhD, Kunio Doi, PhD, Yulei Jiang, PhD, and Xin-Wei Xu, PhD, for helpful discussions. We would like to express our appreciation to Catherine J. Moran for her assistance in data analysis and to Steven Montner, MD, and Carl J. Vyborny, MD, PhD, for their evaluation of the computer-determined lung segmentation contours that was required for baseline normal image selection.

REFERENCES

1. Powell GF, Doi K, Katsuragawa S: Localization of interrib spaces for lung texture analysis and computer-aided diagnosis in digital chest images. Med Phys 15:581-587, 1988

2. Wechsler H, Sklansky J: Finding the rib cage in chest radiographs. Pattern Recog 9:21-30, 1977

3. Sanada S, Doi K, MacMahon H: Image feature analysis and computer-aided diagnosis in digital radiography: Automated delineation of posterior ribs in chest images. Med Phys 18:964-971, 1991

4. Chen X, Doi K, Katsuragawa S, et al: Automated selection of regions of interest for quantitative analysis of lung textures in digital chest radiographs. Med Phys 20:975-982, 1993

5. Xu X-W, Doi K: Image feature analysis for computer-aided diagnosis: Accurate determination of ribcage boundary in chest radiographs. Med Phys 22:617-626, 1995

6. Xu X-W, Doi K: Image feature analysis for computer-aided diagnosis: Detection of right and left hemidiaphragm edges and delineation of lung field in chest radiographs. Med Phys 23:1613-1624, 1996

7. Armato SG, III, Giger ML, MacMahon H: Computerized delineation and analysis of costophrenic angles in digital chest radiographs. Acad Radiol 5:329-335, 1998

8. Sherrier RH, Johnson GA: Regionally adaptive histogram equalization of the chest. IEEE Trans Med Imaging 6:1-7, 1987

9. Cheng D, Goldberg M: An algorithm for segmenting chest radiographs. Proc SPIE 1001:261-268, 1988

10. Sezan MI, Tekalp AM, Schaetzing R: Automatic anatomically selective image enhancement in digital chest radiography. IEEE Trans Med Imaging 8:154-162, 1989

11. Pietka E: Lung segmentation in digital radiographs. J Digit Imaging 7:79-84, 1994

12. Duryea J, Boone JM: A fully automated algorithm for the segmentation of lung fields on digital chest radiographic images. Med Phys 22:183-191, 1995

13. McNitt-Gray MF, Huang HK, Sayre JW: Feature selection in the pattern classification problem of digital chest radiograph segmentation. IEEE Trans Med Imaging 14:537-547, 1995

14. Armato SG, III, Giger ML, MacMahon H: Automated lung segmentation in digitized posteroanterior chest radiographs. Acad Radiol 5:245-255, 1998

15. Kano A, Doi K, MacMahon H, et al: Digital image subtraction of temporally sequential chest images for detection of interval change. Med Phys 21:453-461, 1994

16. Kruger RP, Townes JR, Hall DL, et al: Automated radiographic diagnosis via feature extraction and classification of cardiac size and shape descriptors. IEEE Trans Biomed Eng 19:174-186, 1972

17. Toriwaki J, Suenaga Y, Negoro T, et al: Pattern recognition of chest x-ray images. Comput Graph Image Proc 2:252-271, 1973

18. Hashimoto M, Sankar PV, Sklansky J: Detecting the edges of lung tumors by classification techniques. Proc IEEE Int Conf Patt Recogn 1801:276-279, 1982

19. Lampeter WA, Wandtke JC: Computerized search of chest radiographs for nodules. Invest Radiol 21:384-390, 1986

20. Giger ML, Doi K, MacMahon H, et al: Pulmonary nodules: Computer-aided detection in digital chest images. RadioGraphics 10:41-51, 1990

21. Katsuragawa S, Doi K, MacMahon H, et al: Quantitative computer-aided analysis of lung texture in chest radiographs. RadioGraphics 10:257-269, 1990

22. Nakamori N, Doi K, Sabeti V, et al: Image feature analysis and computer-aided diagnosis in digital radiography: Automated analysis of sizes of heart and lung in chest images. Med Phys 17:342-350, 1990

23. Sanada S, Doi K, MacMahon H: Image feature analysis and computer-aided diagnosis in digital radiography: Automated detection of pneumothorax in chest images. Med Phys 19:1153-1160, 1992

24. Yoshimura H, Giger ML, Doi K, et al: Computerized scheme for the detection of pulmonary nodules: A nonlinear filtering technique. Invest Radiol 27:124-129, 1992

25. Armato SG, III, Giger ML, MacMahon H: Computerized detection of abnormal asymmetry in digital chest radiographs. Med Phys 21:1761-1768, 1994

26. Huang HK, Taira RK: Infrastructure design of a picture archiving and communication system. Am J Roentgenol AJR 158:743-749, 1992

27. Abe K, Doi K, MacMahon H, et al: Computer-aided diagnosis in chest radiography: Preliminary experience. Invest Radiol 28:987-993, 1993

28. Moore DS, McCabe GP: Introduction to the practice of statistics. New York, NY, W.H. Freeman and Company, 1993

29. Metz CE: ROC methodology in radiologic imaging. Invest Radiol 21:720-733, 1986

30. Metz CE, Herman BA, Shen J-H: Maximum likelihood estimation of receiver operating characteristic (ROC) curves from continuously-distributed data. Stat Med 17:1033-1053, 1998